Ken Healy
Vishva Ray*
Lauren J. Willis
Neil Peterman**
John Bartel***
Marija Drndić

Department of Physics and
Astronomy, University of
Pennsylvania, Philadelphia, PA,
USA

Research Article

Fabrication and characterization of nanopores with insulated transverse nanoelectrodes for DNA sensing in salt solution

We report on the fabrication, simulation, and characterization of insulated nanoelectrodes aligned with nanopores in low-capacitance silicon nitride membrane chips. We are exploring these devices for the transverse sensing of DNA molecules as they are electrophoretically driven through the nanopore in a linear fashion. While we are currently working with relatively large nanopores (6–12 nm in diameter) to demonstrate the transverse detection of DNA, our ultimate goal is to reduce the size sufficiently to resolve individual nucleotide bases, thus sequencing DNA as it passes through the pore. We present simulations and experiments that study the impact of insulating these electrodes, which is important to localize the sensing region. We test whether the presence of nanoelectrodes or insulation affects the stability of the ionic current flowing through the nanopore, or the characteristics of DNA translocation. Finally, we summarize the common device failures and challenges encountered during fabrication and experiments, explore the causes of these failures, and make suggestions on how to overcome them in the future.

1 Introduction

Nanopores, nanometer-sized pores in thin membranes, have been studied for close to 20 years now as a potentially revolutionary DNA sequencing method [1–6], promising low-cost, high-throughput, and extremely long read length. The basic concept involves placing a chamber of electrolyte solution on either side of the nanopore and applying a voltage between the chambers. This drives a flux of ions through the pore, which can be measured as a current flowing in the circuit. DNA molecules placed in the cathodic chamber are driven through the pore by their charge, blocking the ionic current as they pass through. With an appropriately sized pore, the DNA molecule is forced to move through in single-file, and thus the current blockage corresponds to the local structure of the DNA molecule along its length, and ultimately its sequence.

However, since the early days of nanopore research, it has been realized that DNA molecules move through the nanopore so fast that any differences in current due the DNA sequence will be swamped by the inevitable noise from the

amplifier electronics and the thermal motion of ions [7]. Two general approaches have been explored to counter this problem. The first is to slow down the DNA molecule, and work based on this approach is today on the cusp of achieving DNA sequencing [8, 9]. The other approach has been to reposition the sensing electrodes. Instead of sensing with macroscopic electrodes on either side of the membrane, translocating DNA is sensed with a pair of nanoelectrodes on the membrane surface, positioned directly on either side of the nanopore aperture. This is shown schematically in Fig. 1A. This so-called "transverse sensing" approach has yet to come close to achieving DNA sequencing, but is still of significant interest as it could enable sequencing without substantially slowing down the DNA molecule.

Research to date has focused almost exclusively on one transverse sensing methodology. That is, to measure the electronic tunneling current between the nanoelectrodes and the modulations in this current for each nucleotide base. However, other sensing approaches are also feasible with a transverse nanoelectrode configuration. For example, with

Correspondence: Professor Marija Drndić, Department of Physics and Astronomy, University of Pennsylvania, 209 S 33rd St, Philadelphia, PA, 19104, USA
E-mail: drndic@physics.upenn.edu
Fax: +1-215-898-2010

**Abbreviation: TEM,** transmission electron microscope

*Current address: Department of Electrical Engineering and Computer Science, University of Michigan, Ann Arbor, MI, USA
**Current address: Department of Physics, Harvard University, Cambridge, MA, USA
***Current address: Department of Physics, Stanford University, Stanford, CA, USA

Colour Online: See the article online to view Figs. 1–4 in colour.
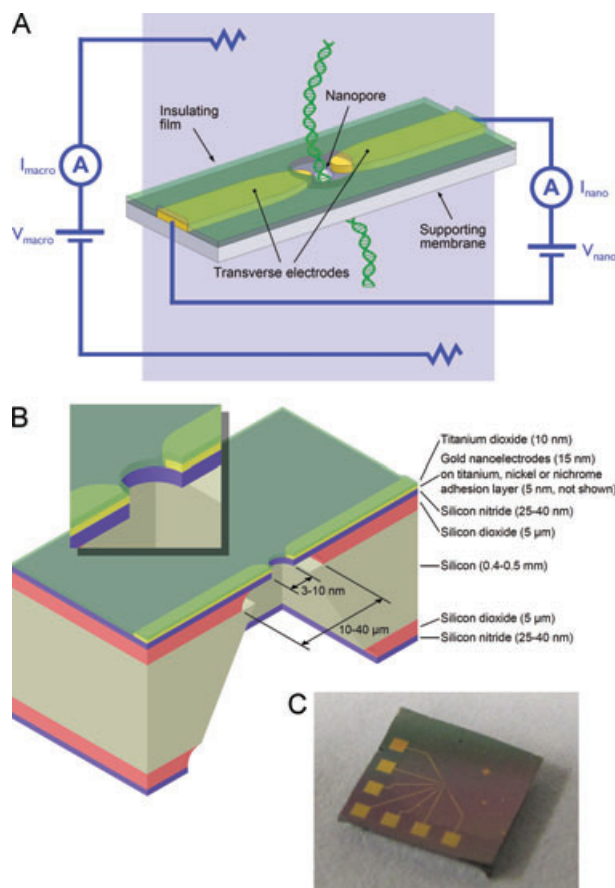
Figure 1. (A) Transverse sensing concept. DNA molecules are driven through the nanopore by an electric field applied via macroscopic electrodes, and the DNA bases modulate the transverse signal between the nanoelectrodes as they pass between them. (B) Diagram showing a cross-section of a silicon nitride membrane chip with a nanopore, nanoelectrodes, and insulation. The inset shows a magnified view of the nanopore area. (C) Photograph of an actual chip, where the contact pads used to interface with the nanoelectrodes can be seen. The titanium dioxide insulation layer is also faintly visible as a pinkish tinge over the connecting traces. It has been removed over the contact pads.

an appropriate electrolyte, an ionic current can flow between the nanoelectrodes, which will be blocked by passing DNA molecules, similar to the traditional nanopore approach described above. Another transverse sensing approach that is beginning to attract interest is detecting modulations in the current flowing through a nanowire or a graphene nanoribbon, as a DNA molecule passes through it or nearby [10–12]. Instead of a transverse nanoelectrode arrangement, nanoelectrodes can also be layered on top of one another, and these sensing geometries are also being explored [13–16].

DNA sequencing based on tunneling current measurements was first explored in theory and simulation [17–23], which suggested that current differences on the order of 0.1–20 pA could be expected. Although tunneling current increases exponentially as the gap between the electrodes and the DNA molecule decreases (for example, [24]), the physical

limitation is that the DNA molecule must be free to move past the electrodes. Lindsay and co-workers have studied this tunneling current in a scanning tunneling microscope [25–31]. They used specially designed adapter molecules that mediate tunneling between the gold scanning tunneling microscope tip and substrate, through the nucleotide base. They have shown that each adenine, guanine, thymine, or cytosine base does modulate the tunneling current in a distinct way. Kawai and co-workers have shown similar results, albeit with less clear distinction between each base, using gold nanoelectrodes without any adapter molecules. They present results with electrodes arranged in a mechanically controllable break junction configuration where the electrodes are freestanding, surrounded by solution [32–34]. They also present, in a separate experiment, a nanopore configuration where the electrodes are embedded in silicon dioxide, with the gap between the nanoelectrodes being the only opening for solution to pass through [35]. However, they did not electrophoretically drive DNA molecules through this gap; they relied on molecules randomly diffusing in and out. Two other groups have also reported transverse detection of DNA molecules [36, 37], but they showed very limited datasets and have yet to follow up on these results. Note that of the experimental approaches discussed in this paragraph [25–37], only [37] is compatible with high-resolution transmission electron microscope (TEM) imaging. As a consequence, there is no way to directly confirm the nanoelectrode spacing, and, more importantly, that there is no debris near the electrodes and their shape is as anticipated.

In this article, we present our work on nanopores in silicon nitride membranes with aligned nanoelectrodes, for transverse sensing across the pore aperture. This has involved fabricating these devices, imaging them by transmission electron microscopy, and testing their electrical characteristics in salt solution. We discuss the need to insulate these nanoelectrodes, while optionally keeping their tips exposed, and describe and evaluate the process we developed to achieve this. We also explore whether the presence of nanoelectrodes and insulation affects nanopore stability or DNA translocation, as observed in the ionic current signal measured using macroscopic electrodes. Finally, we summarize the failure modes of these nanopore devices during fabrication and experiments, discuss the challenges these failures pose to realizing successful and reproducible transverse measurements with nanoelectrodes, and give recommendations on how best to overcome these failures in the future.

2 Materials and methods

2.1 Silicon nitride membrane fabrication

The fabrication of silicon nitride membranes suspended on silicon support "chips," for example, as described in [38], is a standard process. We used a modified version of this process to produce silicon nitride membranes (10–40 μm square) with a 5-μm silicon dioxide layer between the silicon nitride

and silicon for reduced capacitance. The process modifications involved growing 5 μm of silicon dioxide, by wet thermal oxidation, on each side of the (100) silicon wafer before low-stress (200–300 MPa) silicon nitride deposition, and additionally etching through these silicon dioxide layers with 6:1 buffered hydrofluoric acid (Transene, Danvers, MA, USA). Please note that appropriate safety precautions should be taken and extreme care used when working with hydrofluoric acid. A few drops of Triton X-100 surfactant (Sigma Aldrich, St. Louis, MO, USA) per liter of buffered hydrofluoric acid were added to reduce the surface tension and avoid trapped air bubbles. It was necessary to vapor prime the wafer with hexamethyldisilazane before spincoating photoresist, for both buffered hydrofluoric acid etch steps, to prevent the photoresist from peeling during the etch. A side effect of the thick silicon dioxide layer, due to its compressive stress, is that the silicon nitride membranes are not flat, but are deformed slightly upwards. The maximum deformation occurs at the center and is approximately 1% of the membrane width. Silicon dioxide growth and silicon nitride deposition were provided as a service by the Cornell Nanoscale Science and Technology Facility, Ithaca, NY, USA. All subsequent fabrication was carried out by the authors at the University of Pennsylvania.

2.2 Nanoelectrode fabrication

A two-stage process was used to fabricate nanoelectrodes, and contacts to connect to them with. The first step was to deposit the nanoelectrodes and fine connecting traces going to the edge of the silicon nitride membrane. This was achieved by a standard lift-off process. Briefly, the pattern to be deposited was defined in C2 950 PMMA resist (Microchem, Newton, MA, USA) by electron beam lithography (ELS-7500EX, Elionix, Tokyo, Japan), an adhesion layer of nickel, titanium, or nichrome (5 nm) followed by a layer of gold (15 nm) was deposited on top by thermal evaporation (custom-built system, although any standard commercial evaporator will suffice), and then the resist was "lifted-off" using acetone, leaving metal only in the pattern defined by the photoresist. Next, contact pads, and coarse connecting traces to connect to the nanoelectrodes, were deposited using a similar lift-off process, using optical lithography (MA4 mask aligner, Süss Microtec, Sunnyvale, CA, USA), instead of electron beam lithography. The photoresist used was NR7 (Futurrex, Franklin, NJ, USA).

2.3 Nanoelectrode insulation

The nanoelectrodes were insulated by atomic layer deposition. A Savannah 200 system (Cambridge Nanotech, Cambridge, MA, USA) was used to deposit 10 nm of titanium dioxide over the entire silicon nitride membrane chip. Subsequently, the titanium dioxide covering the contact pads was plasma etched away (Planar Etch II or PE II-A, Technics West, San Jose, CA, USA; $SF_6 + O_2$ mixture, approximately

600 mTorr pressure, 150 W, 1–3 min) so that electrical connections could be made. A second silicon nitride membrane chip was placed on top of the first chip to mask the areas not to be etched.

2.4 Nanopore drilling and nanoelectrode shaping

The silicon nitride membrane chip with electrodes and insulation was then inserted into a JEOL 2010F field-emission TEM (JEOL USA, Peabody, MA, USA). The nanoelectrode tips were fine-tuned, if necessary, by nanosculpting them using the transmission electron beam ablation lithography technique developed in our lab [39]. This was done if the gap between them was not sufficient, or the tips needed to be sharpened or exposed to solution. Then, a nanopore was drilled between the electrodes by the usual electron beam drilling approach [40]. If the nanopore is drilled to intersect the electrode tips, the insulation will be removed there, allowing electrochemical conduction. For both transmission electron beam ablation lithography and nanopore drilling, the microscope was operated at 200 kV in standard TEM mode, with a 150-μm condenser aperture and maximum beam convergence angle (α1 mode). At the start of each TEM session, the electron beam was aligned using the manufacturer-specified high-resolution alignment procedure while imaging a holey carbon sample. After loading each silicon nitride membrane chip, the alignment was also fine-tuned. This was done on an unimportant area of the membrane, to avoid any damage to the nanoelectrodes. To ablate material, the target region was centered on the viewing screen at 500 000–1 000 000 times magnification, and the beam condensed to the tightest spot possible. Ablation occurs on the order of seconds for most metals, and minutes for silicon nitride, but depends on the microscope conditions and the particular material and its thickness. Ablation progress can be observed both as an increase in the beam current transmitted through the sample, and visually on the microscope's phosphor imaging screen; although the beam is maximally condensed, the intense central spot is surrounded by a weak halo, sufficient to view the ablation progress. When the desired result was achieved, ablation was stopped by decondensing the beam. To ablate more than a single spot, the beam was manually shifted to ablate the desired pattern. Beam shift was also used to compensate for mechanical drift of the sample stage, which was often significant during long ablation operations. In contrast to lighter metals such as silver, nickel, chrome, and aluminum, gold is not substantially ablated by the 200 kV electron beam due to its high atomic weight. Instead, beam exposure prompts the gold to crystallize. We exploit this behavior to nanosculpt gold by directing the beam at an area adjacent to where material is to be removed. The resulting crystallization "pulls in" the gold, away from the target area. Note that a standard JEOL 2010F sample holder can only accommodate approximately 3 × 3 mm samples. We modified this holder by milling a larger recess to accommodate 5 × 5 mm silicon nitride membrane chips. The chips are placed membrane-side down into

this holder so that the membrane is closest to the center of the microscope's focal range.

2.5 Ionic current measurements, DNA translocation experiments, and nanoelectrode measurements

The nanopore chips were treated by UV/ozone (PSDP-UVT, Novascan, Ames, IA, USA; 80°C, 15 min each side) to facilitate wetting, and then mounted in a custom-made PDMS measurement cell. Oxygen plasma treatment (Technics PE II-A, Technics West; 50 W, approximately 400 mT, 5 min, with the chip elevated to expose both sides) gave similar results. The cell had sub-millimeter width fluidic channels to limit the area of solution in contact with the chip surface, and thus the capacitance. The laminar solution flow imposed by these channels, together with the hydrophilic nature of PDMS, make the occurrence of trapped air bubbles rare. The cell channels were filled with a solution of 1 M KCl, 10 mM Tris, 1 mM EDTA at pH 8.5–9.0 (all chemicals from Sigma Aldrich). For DNA translocation measurements, 15 kbp Fermentas NoLimits ds-DNA fragments (Fermentas, Glen Burnie, MD, USA) were also added to the solution on the cathodic side. Ag/AgCl pellet electrodes (A-M Systems, Sequim, WA, USA) made electrochemical connection to the solution, and an HEKA EPC10 triple channel patch clamp amplifier (HEKA Instruments, Bellmore, NY, USA) was used to apply voltage and measure and digitize current. Data were filtered using a 10 kHz 5-pole Bessel filter built into the EPC10 and digitized at 50 kHz. Custom software to record and analyze the data was written in LabVIEW (National Instruments, Austin, TX, USA). For nanoelectrode measurements, the contact pads on the silicon nitride membrane chip were bonded to a custom-designed 0.35-mm thickness printed circuit board (OurPCB, Shijiazhuang, China) using conductive silver paste. This enabled simultaneous fluidic and electrical connection to the chip. The circuit board plugs into a flat flexible cable connector on another circuit board, which is connected to the second channel of the EPC10 amplifier.

3 Results and discussion

Figure 1B shows a schematic of the silicon nitride membrane chip with a nanopore and insulated nanoelectrodes. Figure 1C is a photograph of an actual 5×5 mm^2 chip where the contact pads and traces that connect to the nanoelectrodes can be seen. The titanium dioxide insulation layer is also faintly visible as a pinkish tinge over the connecting traces. It has been removed over the contact pads.

Insulating the nanoelectrodes is crucial to localize sensing to the nanoelectrode gap when measuring in electrolyte solution. In theory, with perfectly pure solutions, and pure gold electrodes, no electrochemical reactions should take place at the voltages used (± 100 mV). However, due to impurities in the solutions and electrodes, a large leakage current does flow (tens of nA at 25 mV), relative to that expected

to flow just between the electrode tips. Thus, the current flowing between areas of the electrodes away from the tips swamps the signal of interest. Figure 2A–C shows finite element simulations of current density, for a potential difference of 1 V applied between the electrodes, in a solution of conductivity 1 S/m. The nanopore is 5 nm in diameter, and electrodes are 2-nm high, 5-nm wide, and 2-μm long, with flat faces terminating at the pore edge. Where present, the insulation is 3-nm thick. These simulations were carried out using COMSOL Multiphysics (COMSOL, Burlington, MA, USA). Without insulation (Fig. 2A, and dashed curve in Fig. 2C), the current density decays very slowly with distance from the nanoelectrodes. In fact, the fraction of the total current that flows through a rectangle the size of the electrode cross-section (see Fig. 2D) is negligible (<0.3%). With insulation (Fig. 2B and solid curve in Fig. 2C), the situation is quite different. The current density decays rapidly, and 25% of the total current flows through the same rectangle. The insulation must be thick enough to ensure uniform and complete coverage and sufficiently high resistance, but thin enough not to interfere with nanopore drilling. Ten nanometers has been sufficient in our experience. We were not able to achieve complete coverage with thinner layers, but this could likely be addressed by optimizing our atomic layer deposition (ALD) process. Figure 2E shows a contrast-enhanced TEM image of insulated electrodes, where the titanium dioxide can be distinguished as a halo around the electrodes. This halo is not present without insulation. We test the impact of the insulation by measuring the leakage current that flows from one of the nanoelectrodes to a macroscopic electrode inserted in the solution (see the inset in Fig. 2F). Figure 2F highlights that the leakage current drops by several orders of magnitude to a few pA for insulated electrodes, over the voltage range tested.

Importantly, these nanopore devices with insulated nanoelectrodes can be produced reliably. Figure 3A–F shows TEM images of a range of devices with nanoelectrodes spaced from 2.5 to 30 nm. We are aware that the distance between the nanoelectrodes in most of these devices is larger than that necessary to give a detectable tunneling current signal. We have demonstrated the fabrication of small gaps down to 1.5 nm [39], but for this work on developing and refining the fabrication and experimental processes, it is simply quicker and easier to work with somewhat larger gaps as they are simpler to fabricate. In addition, we have fabricated multiple nanopores and nanoelectrodes on one silicon nitride membrane, for example, for sensing the same DNA sample in parallel. Figure 3G shows a device with 12 pairs of nanoelectrodes.
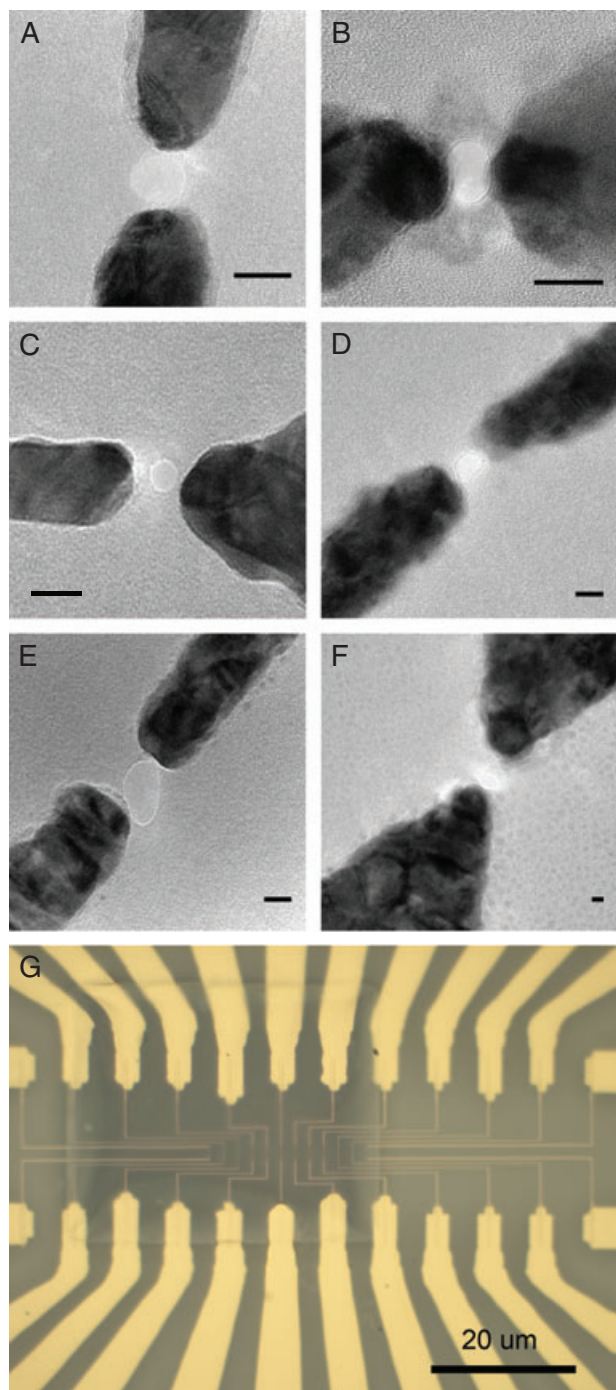
We have tested to see if the presence of nanoelectrodes and insulation affect pore stability, as observed by measuring the ionic current between macroscopic electrodes. Figure 4A shows the conductance of three different nanopores over a period of 60 min, one with insulated nanoelectrodes, one with bare nanoelectrodes, and the other in a bare silicon nitride membrane. All nanopores were approximately 6 nm in diameter. For all cases, it can be seen that the open-pore
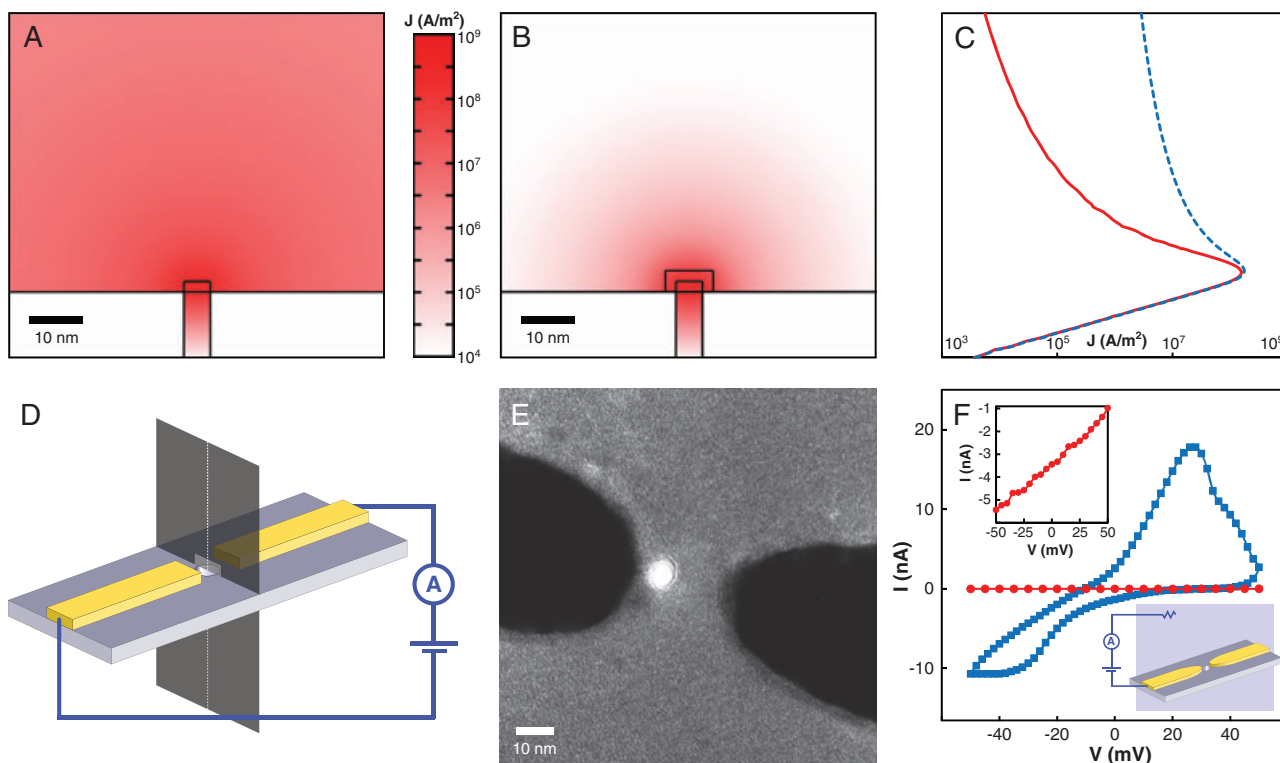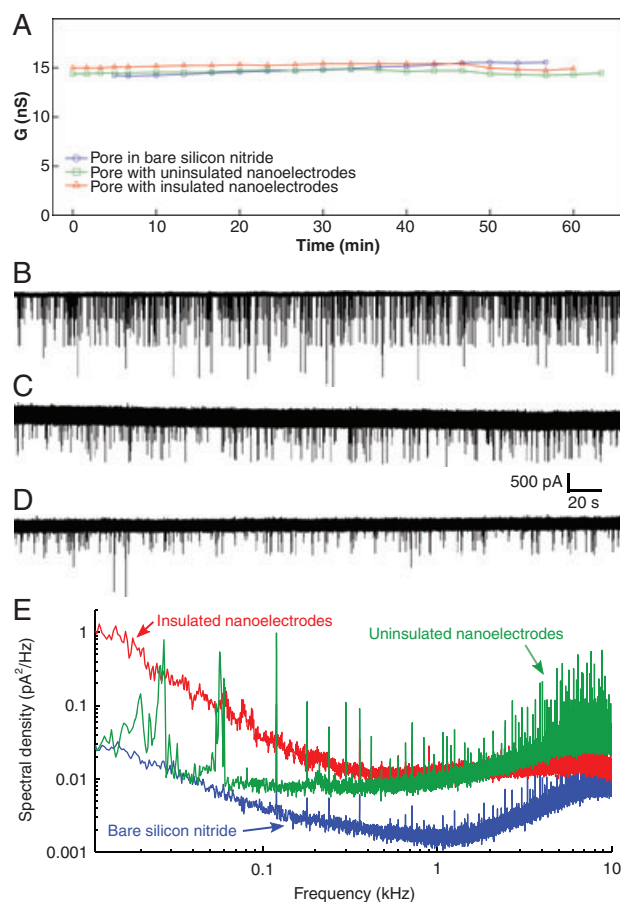
Figure 2. (A–C) Finite element simulations of the current density for a potential difference of 1 V between the nanoelectrodes, without (A, dashed line in C) and with (B, solid line in C) insulation. The nanopore is 5 nm in diameter, the electrodes are 2-nm high, 5-nm wide, and have flat faces terminating at the pore edge. Each nanoelectrode is 2-μm long. The insulation (if present) is 3-nm thick and covers all but the end face of the nanoelectrodes. The solution conductivity is 1 S/m. Note that the vertical axis is the same for (A–C). (D) Diagram showing how plots (A–C) are oriented. (A, B) are plots on the dark plane intersecting the membrane. The lighter rectangle on this plane is a projection of the electrode cross-section. The fraction of the total current flowing through this rectangle is quoted in the text. The curves in (C) are plots on the dashed line running along the nanopore axis. (E) TEM image of nanoelectrodes with titanium dioxide insulation. The contrast of this image is amplified to highlight the titanium dioxide layer. (F) Leakage current for uninsulated (blue squares) and insulated (red circles) electrodes, with the low leakage in the latter case highlighted in the left inset. The right inset shows the measurement configuration. This measurement was carried out in 1 M KCl, 10 mM Tris, 1 mM EDTA, pH 8.5.

conductance remains constant around 15 nS, and there are no appreciable changes in stability over this period, which is much longer than the duration of typical nanopore sensing experiments (1–20 min). Similarly, DNA translocations are not affected. Figure 4B and D presents ionic current recordings taken using macroscopic electrodes. These show DNA translocations through each pore, again showing that there are no significant changes with electrodes or insulation, apart from the differences that are evident in the baseline noise level. We observe that nanopores with insulated nanoelectrodes exhibit higher noise in the ionic current signal measured with macroscopic electrodes, compared to nanopores without nanoelectrodes. With bare nanoelectrodes, the noise is higher still. This is expected because the presence of nanoelectrodes increases the capacitance from one side of the membrane to the other. This capacitance scales the voltage noise of the amplifier electronics, which then contributes to the noise in the measured current. Therefore, higher capacitance means higher noise. Nanopore membranes can be reasonably approximated as parallel plate capacitors, whose capacitance is proportional to the plate area, and inversely proportional to the thickness of dielectric between the plates. The silicon support corresponds to one of the parallel plates, the silicon dioxide and silicon nitride layers are the dielectric, and the solution forms the other plate. (The silicon nitride membrane with no underlying silicon dioxide in the center of the chip can be ignored in this approximation, because its area is small compared to the total area). Without nanoelectrodes, the capacitor plate area corresponds to the area of solution in contact with the silicon nitride surface, in our case approximately 0.7 mm^2. However, with uninsulated nanoelectrodes, the solution is now electrically connected to the electrodes and their associated connecting traces and contact pads, which have a significantly larger area than that wetted by solution. Therefore, the capacitor plate area has expanded and the capacitance, and thus noise, goes up. With insulated electrodes, the additional capacitance due to the traces and contact pads outside the wetted area is in series with the capacitance from the solution through the insulation into the electrodes. As series capacitances add reciprocally, this will result in a smaller increase in capacitance and noise compared to the case of bare electrodes. The impact of this capacitance can be seen more clearly in power spectral density plots. Figure 4E shows power spectra of the ionic current

Figure 4. The presence of nanoelectrodes and insulation do not affect the ionic current through the nanopore (A), or the characteristics of DNA translocation (B–D). (B) Nanopore in a bare silicon nitride membrane without nanoelectrodes, (C) nanopore with uninsulated nanoelectrodes, (D) nanopore with insulated nanoelectrodes. (E) Noise power spectral density plots of the ionic current measured without DNA, for the same nanopore devices as in (A–D). The left-hand regions of the plots that decrease with frequency are $1/f$ noise, commonly associated with fluctuations in wetting of the nanopore surface. The right-hand regions that increase with frequency are due to the voltage noise of the amplifier scaled by the membrane capacitance. Note that the sharp spikes in these plots are all due to external interference, mainly from switching power supplies in computer equipment. Each spike is confined to a very narrow frequency band, so the spikes do not contribute significantly to the total noise. All measurements were carried out with 120 mV bias voltage, using 1 M KCl, 10 mM Tris, 1 mM EDTA, at pH 8.5–9.0. For DNA translocation experiments, 15 kbp DNA was added to this solution.

Figure 3. (A–F) TEM images of a range of nanopore-nanoelectrode devices. The distance between the nanoelectrodes in these devices ranges from 2.5 to 30 nm. Dark areas are gold (on a nickel, titanium, or nichrome adhesion layer), lighter gray is the silicon nitride membrane, and the light circles between the gold nanoelectrodes are nanopores through the silicon nitride membrane. All scale bars are 10 nm. (G) Optical microscope image showing a silicon nitride membrane with 12 pairs of nanoelectrodes and associated connecting traces.

signal measured with macroscopic electrodes for the same three nanopore devices in Fig. 4A–D. These were control measurements without any DNA, so the ionic current was steady, without any translocation events. The capacitance-scaled amplifier voltage noise is responsible for the rise in noise power with increasing frequency on the right-hand side of these plots. Higher noise in this region corresponds to higher capacitance, so, as expected, the noise is highest with uninsulated nanoelectrodes and lowest for the nanopore in

a bare silicon nitride membrane. Note that the "1/*f*" sloped sections on the left-hand side of these plots are not related to the capacitance. High 1/*f* noise is commonly associated with poor wetting of the nanopore surface [41–44]. Given the logarithmic nature of the plot, this 1/*f* component does not significantly influence the total noise, which was confirmed by computing the total rms (root mean square) noise as the integral of the spectral density with respect to frequency (not shown).

Fabricating nanopore-nanoelectrode devices and translocating DNA molecules through them is a complex process involving many steps. Device failure can and does occur at many points in the process and resulted in a very low yield of successful DNA translocation measurements. In addition, this low yield has prevented us to date from characterizing the transverse signal between the nanoelectrodes, or carrying out transverse measurements of DNA translocation. Over a 2-year period, we have fabricated over 300 of these devices. Approximately 15% of these were intact at the end of the fabrication process, as diagnosed by TEM and optical microscope imaging. Of these intact devices, none yielded reliable measurements of the transverse signal between the nanoelectrodes. The devices either failed during the experiment setup or during control measurements with macroscopic electrodes, or the nanoelectrode signal was not stable. We have not yet encountered enough of many of these failures to make statistically significant conclusions, so the following can be regarded as anecdotal observations. We see four broad classes of device failure: membrane rupture, lower (and often noisier) ionic current than would be expected for the pore's diameter and membrane thickness, devices that have expected ionic current but do not show any DNA translocation events, and devices that pass all other tests, but exhibit unstable or invalid nanoelectrode current. Membrane rupture can occur during device fabrication and during experiments. The ruptures during fabrication can be divided into two categories, the first being breakage due to mechanical shock. This is evident as jagged silicon nitride edges where the rupture occurred, much like broken glass, as shown in Fig. 5A. The second is electrostatic discharge. This occurs centered at the nanoelectrode tips and is characterized by ruptures several microns in diameter with rounded edges that could be described as melted or burned (Fig. 5B and C). It is harder to analyze ruptures during experiments because removing the device from the measurement cell, cleaning it, and drying it is likely to cause further damage. However, based on the conductance, we do observe a range of rupture sizes. Mechanical ruptures can generally be avoided by careful handling, although there are more opportunities for failure with nanoelectrodes because of the additional processing steps required to fabricate them. Electrostatic discharge is more difficult to handle. We have had success in avoiding the latter during fabrication by connecting the nanoelectrode contact pads to each other with a narrow trace at the lithography stage. This ensures the electrodes are at the same potential, so that electrostatic discharge will not occur from one to the other. This connecting trace is then cut just before inserting the device into the measure-
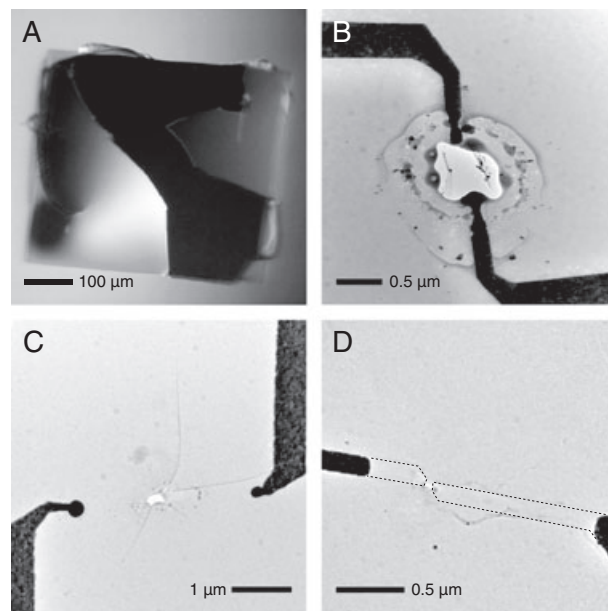
Figure 5. (A) Optical microscope image of a silicon nitride membrane that ruptured due to mechanical shock. This membrane is much larger than those used for nanopore experiments. It is shown here because its size illustrates the characteristics of rupture very clearly, but smaller membranes rupture in the same way. (B, C) TEM images of ruptures caused by electrostatic discharge between nanoelectrode tips. Note the difference between the smooth edge of the rupture characteristic of electrostatic discharge, compared to the jagged edge associated with mechanical shock. In the case of electrostatic discharge, the membrane may also have fractures in the radial direction, as in (C). (D) TEM image of a nanopore-nanoelectrode device after measurement in solution that did not rupture due to mechanical shock or electrostatic discharge, but where the nanoelectrode tips have disappeared. The dashed lines show the original footprints of the nanoelectrodes.

ment cell. The causes of lower than expected ionic current are not yet fully understood, but this has been observed previously in nanopores and is generally associated with poor wetting of the nanopore surface [41–44], perhaps due to organic contaminants on the surface rendering it more hydrophobic. For silicon nitride nanopores without nanoelectrodes, aggressive cleaning in hot piranha solution [44, 45] reliably resolves the issue and restores the ionic current to the expected value.

Caution: Piranha is a strong oxidizer that reacts violently with most organic materials. Unfortunately, piranha solution destroys our nanoelectrodes, and we have not found a similarly successful cleaning method. For devices that showed as expected ionic current, but no DNA translocation events, we do not yet have any explanation. We can only point out that this absence of DNA translocation events does not occur for nanopores without nanoelectrodes. Finally, for the few devices with which we observed DNA translocations and that did not rupture before taking a nanoelectrode measurement, the nanoelectrode signal was not reliable. We observed cases where the signal fluctuated wildly, where the nanoelectrode current increased steadily with time, or where the current

increased steadily to a plateau that was much larger than could be expected for the exposed area of gold at the electrode tips [46]. We also saw cases where the current was steady at similarly large current for the duration of the measurement. While we do not have any conclusive explanation for these results, it seems likely that either there is some remaining metal or other electrically conductive residue connecting the nanoelectrodes, or that there were gaps in the insulation layer for these particular devices. We also took postexperiment TEM images of these devices. In the majority of cases, we saw that the nanoelectrode tips had disappeared (Fig. 5D) or peeled from the surface of the membrane, they had been thinned significantly, or they had migrated away from the nanopore. Not enough devices survived to this point to discern any correlation between the observed nanoelectrode signals and what was observed in the postexperiment TEM images.

For those wishing to pursue this direction of research, we would emphasize that achieving a reasonable fabrication yield is crucial. Low yield makes it difficult to isolate whether experimental failures are due to fabrication issues, or more fundamental problems with the device or experiment design. Low device yield is also very time-consuming and demoralizing for those carrying out the research. For reasonable yield, it is important to minimize mechanical shock and electrostatic buildup. Mechanical shock is generally not an issue due to the robustness of silicon nitride membrane chips, but if it occurs, it can be easily identified by optical inspection, and eliminated by gentler treatment of the chips. As an aside, for silicon nitride membranes with an underlying silicon dioxide layer where the membrane is not flat due to the stress in the oxide, we would advise against depositing thick (>100 nm) metal traces on the membrane, as the traces will distort the membrane and may cause it to rupture. To minimize the chances of membrane rupture due to electrostatic discharge, we recommend connecting the nanoelectrode contact pads to each other to keep them at the same potential, as described above. An ionizing air blower, for example, Simco-Ion Model 5802i (Simco-Ion, Hatfield, PA, USA), may also help to prevent electrostatic buildup. In addition to fabrication yield, surface contamination is another major issue that has prevented successful nanoelectrode measurements. While we do not have absolute proof that surface contamination is the cause of lower than expected ionic current or excessive ionic current noise in nanopore devices, it is well known that these problems are eliminated by cleaning with piranha solution. While we have yet to find a cleaning method of similar effectiveness that is compatible with metal nanoelectrodes, we do note that these problems are reduced when the nanopore devices are subjected to rapid thermal annealing (MILA-5000, ULVAC Technologies, Methuen, MA, USA; ramp to 350°C in 1 min, hold at 350°C for 1 min, then allow to cool, all in a nitrogen forming gas atmosphere) and/or plasma cleaning (Solarus Model 950, Gatan, Warrandale, PA, USA; 1 min, 6.4 sccm H_2, 27.5 sccm O_2, 70 mTorr, 50 W) directly after removal from the TEM, and then stored in 70% ethanol until they are used in an experiment.

4 Concluding remarks

We have fabricated insulated nanoelectrodes on low-capacitance silicon nitride membranes and drilled nanopores between them. Our simulations show that nanoelectrodes must be insulated, apart from their tips, to localize the sensing region, for measurements in electrolyte solution. We accomplished this insulation by atomic layer deposition and show leakage current measurements to prove that it works. By performing ionic current measurements using macroscopic electrodes, we have demonstrated that the presence of nanoelectrodes and insulation does not affect the stability of the ionic current flowing through these pores, nor does it affect the characteristics of DNA translocation. However, device failure during fabrication and experiments has been a significant issue. This has to date prevented us from reliably and reproducibly measuring current between the nanoelectrodes or studying their response to translocating DNA molecules. We have summarized the types of device failure we have encountered, discussed the causes, where known, and made recommendations on how those wishing to pursue this direction of research can minimize these failures.

The authors have declared no conflict of interest.

5 References

[1] Healy, K., *Nanomedicine* 2007, *2*, 459–481.

[2] Healy, K., Schiedt, B., Morrison, A. P., *Nanomedicine* 2007, *2*, 875–897.

[3] Dekker, C., *Nat. Nanotechnol.* 2007, *2*, 209–215.

[4] Branton, D., Deamer, D. W., Marziali, A., Bayley, H., Benner, S. A., Butler, T., Di Ventra, M., Garaj, S., Hibbs, A., Huang, X., Jovanovich, S. B., Krstić, P. S., Lindsay, S., Sean Ling, X., Mastrangelo, C. H., Meller, A., Oliver, J. S., Pershin, Y. V., Ramsey, J. M., Riehn, R., Soni, G. V., Tabard-Cossa, V., Wanunu, M., Wiggin, M., Schloss, J. A., *Nat. Biotechnol.* 2008, *26*, 1146–1153.

[5] Venkatesan, B. M., Bashir, R., *Nat. Nanotechnol.* 2011, *6*, 615–624.

[6] Wanunu, M., *Phys. Life Rev.* 2012, *9*, 125–158.

[7] Deamer, D. W., Akeson, M., *Trends Biotechnol.* 2000, *18*, 147–151.

[8] Cherf, G. M., Lieberman, K. R., Rashid, H., Lam, C. E., Karplus, K., Akeson, M., *Nat. Biotechnol.* 2012, *30*, 344–348.

[9] Manrao, E. A., Derrington, I. M., Laszlo, A. H., Langford, K. W., Hopper, M. K., Gillgren, N., Pavlenok, M., Niederweis, M., Gundlach, J. H., *Nat. Biotechnol.* 2012, *30*, 349–354.

[10] Xie, P., Xiong, Q., Fang, Y., Qing, Q., Lieber, C. M., *Nat. Nanotechnol.* 2012, *7*, 119–125.

[11] Nelson, T., Zhang, B., Prezhdo, O. V., *Nano Lett.* 2010, *10*, 3237–3242.

[12] Saha, K. K., Drndić, M., Nikolić, B. K., *Nano Lett.* 2012, *12*, 50–55.

[13] Polonsky, S., Rossnagel, S., Stolovitzky, G., *Appl. Phys. Lett.* 2007, *91*, 153103.

[14] Harrer, S., Ahmed, S., Afzali-Ardakani, A., Luan, B., Waggoner, P. S., Shao, X., Peng, H., Goldfarb, D. L., Martyna, G. J., Rossnagel, S. M., Deligianni, L., Stolovitzky, G. A., *Langmuir* 2010, *26*, 19191–19198.

[15] Harrer, S., Waggoner, P. S., Luan, B., Afzali-Ardakani, A., Goldfarb, D. L., Peng, H., Martyna, G., Rossnagel, S. M., Deligianni, L., Stolovitzky, G. A., *Nanotechnology* 2011, *22*, 275304.

[16] Jiang, Z., Mihovilovic, M., Chan, J., Stein, D., *J. Phys.: Condens. Matter* 2010, *22*, 454114.

[17] Zwolak, M., Di Ventra, M., *Nano Lett.* 2005, *5*, 421–424.

[18] Lagerqvist, J., Zwolak, M., Di Ventra, M., *Nano Lett.* 2006, *6*, 779–782.

[19] Zhang, X.-G., Krstić, P. S., Zikić, R., Wells, J. C., Fuentes-Cabrera, M., *Biophys. J.* 2006, *91*, L04–L06.

[20] Lagerqvist, J., Zwolak, M., Di Ventra, M., *Biophys. J.* 2007, *93*, 2384–2390.

[21] Meunier, V., Krstić, P. S., *J. Chem. Phys.* 2008, *128*, 041103.

[22] Krems, M., Zwolak, M., Pershin, Y. V., Di Ventra, M. *Biophys. J.* 2009, *97*, 1990–1996.

[23] Chen, X., Rungger, I., Pemmaraju, C. D., Schwingenschlogl, U., Sanvito, S., *Phys. Rev. B.* 2012, *85*, 115436.

[24] Postma, H. W. Ch., *Nano Lett.* 2010, *10*, 420–425.

[25] He, J., Lin, L., Zhang, P., Lindsay, S., *Nano Lett.* 2007, *7*, 3854–3858.

[26] He, J., Lin, L., Zhang, P., Spadola, Q., Xi, Z., Fu, Q., Lindsay, S., *Nano Lett.* 2008, *8*, 2530–2534.

[27] Chang, S., He, J., Kibel, A., Lee, M., Sankey, O., Zhang, P., Lindsay, S., *Nat. Nanotechnol.* 2009, *4*, 297–301.

[28] Chang, S., He, J., Lin, L., Zhang, P., Liang, F., Young, M., Huang, S., Lindsay, S., *Nanotechnology* 2009, *20*, 185102.

[29] Chang, S., Huang, S., He, J., Liang, F., Zhang, P., Li, S., Chen, X., Sankey, O., Lindsay, S., *Nano Lett.* 2010, *10*, 1070–1075.

[30] Huang, S., He, J., Chang, S., Zhang, P., Liang, F., Li, S., Tuchband, M., Fuhrmann, A., Ros, R., Lindsay, S., *Nat. Nanotechnol.* 2010, *5*, 868–873.

[31] Huang, S., Chang, S., He, J., Zhang, P., Liang, F., Tuchband, M., Li, S., Lindsay, S., *J. Phys. Chem. C* 2010, *114*, 20443–20448.

[32] Tanaka, H., Kawai, T., *Nat. Nanotechnol.* 2009, *4*, 518–522.

[33] Tsutsui, M., Taniguchi, M., Yokota, K., Kawai, T., *Nat. Nanotechnol.* 2010, *5*, 286–290.

[34] Tsutsui, M., Matsubara, K., Ohshiro, T., Furuhashi, M., Taniguchi, M., Kawai, T., *J. Am. Chem. Soc.* 2011, *133*, 9124–9128.

[35] Tsutsui, M., Rahong, S., Iizumi, Y., Okazako, T., Taniguchi, M., Kawai, T., *Sci. Rep.* 2011, *1*, 46.

[36] Liang, X., Chou, S. Y., *Nano Lett.* 2008, *8*, 1472–1476.

[37] Ivanov, A. P., Instuli, E., McGilvery, C. M., Baldwin, G., McComb, D. W., Albrect, T., Edel, J. B., *Nano Lett.* 2011, *11*, 279–285.

[38] Grant, A. W., Hu, Q.-H., Kasemo, B., *Nanotechnology* 2004, *15*, 1175–1181.

[39] Fischbein, M. D., Drndić, M., *Nano Lett.* 2007, *7*, 1329–1337.

[40] Storm, A. J., Chen, J. H., Ling, X. S., Zandbergen, H. W., Dekker, C., *Nat. Mater.* 2003, *2*, 537–540.

[41] Chen, P., Mitsui, T., Farmer, D. B., Golovchenko, J., Gordon, R. G., Branton, D., *Nano Lett.* 2004, *4*, 1333–1337.

[42] Smeets, R. M. M., Keyser, U. F., Wu, M. Y., Dekker, N. H., Dekker, C., *Phys. Rev. Lett.* 2006, *97*, 088101.

[43] Danelon, C., Santschi, C., Brugger, J., Vogel, H., *Langmuir* 2006, *22*, 10711–10715.

[44] Tabard-Cossa, V., Trivedi, D., Wiggin, M., Jetha, N. N., Marziali, A., *Nanotechnology* 2007, *18*, 305505.

[45] Wanunu, M., Meller, A., *Nano Lett.* 2007, *7*, 1580–1585.

[46] Tuchband, M., He, J., Huang, S., Lindsay, S., *Rev. Sci. Instrum.* 2012, *83*, 015102.